CO2 reduction on post-transition metals and their alloys: an industrial approach

Pavesi, D.

Citation

Pavesi, D. (2022, April 20). *CO2 reduction on post-transition metals and their alloys: an industrial approach*. Retrieved from https://hdl.handle.net/1887/3284964

7

Electrochemical CO_2 reduction on gas diffusion electrodes: enhanced selectivity of In-Bi bimetallic particles and catalyst layer optimization through a Design of Experiment approach

This chapter is based on the article:

Philips, M. F., Pavesi, D., Wissink, T., Figueiredo, M., Gruter, G. J. M., Koper, M. T. M., Schouten, K. J. P. Electrochemical CO_2 reduction on gas diffusion electrodes: enhanced selectivity of In-Bi bimetallic particles and catalyst layer optimization through a Design of Experiment approach. ACS Appl. Energy Mater. **accepted**

The article is based on equal contribution by Pavesi, D. and Philips, M. F.

Abstract

Scaling up the CO_2 electroreduction technology to industrial size will require, among other things, to maximize selectivity at high current densities and increase the catalyst lifetime. We show here that InBi electrocatalysts provide enhanced selectivity compared to pure In and Bi and that proper formulation of the catalyst layer can have a profound impact on the performance of Gas Diffusion Electrode electrolyzers. The best performing electrodes screened in this study show nearly 100% faradaic yield at current densities up to 400 mA/cm^2 for two hours. Additionally, one electrode was shown to operate at a current density of 200 mA/cm^2 for 48 hours at a faradaic yield of 85% and remained operating with a faradaic yield above 50% for 124 hours.

7.1 Introduction

Typically, catalysts based on metals such as Sn, In, Pb, Hg and Bi are used for the electrochemical reduction of CO_2 to formate as they attain a high faradaic yield.[1] High current densities are obtained by using Gas Diffusion Electrode (GDE) configurations. GDEs are able to achieve high faradaic yields at high current densities because they overcome mass transport limitations arising from the low solubility of CO_2 in aqueous electrolytes.[2] However, GDEs are much more complex electrodes than a typical 3D metallic electrode and there has been limited optimization and stability studies for this reaction.[3]

A GDE consists of a gas diffusion layer (GDL) and a catalyst layer. Both of these layers can affect the performance of the GDE and should be considered for total optimization of the electrode. The effect of the GDL has been hardly studied in this reaction while the catalyst layer characteristics have received the most attention. The type of binder used in the catalyst layer has been shown to give various performances of GDEs.[3] The amount of catalyst supported on carbon and the binder amount in the catalyst layer have also been scarcely studied for this reaction. Furthermore, most published results for this reaction have a run time of less than eight hours, and consequently, the stability of GDEs for this reaction has not been well assessed.

In this chapter, we provide a rationale for the enhanced performance of Avantium's patented InBi electrocatalyst[4] by comparing it to pure In and Bi catalysts synthesized in the same way. Our findings suggest that the slight improvement in performance is due to an increase in the fraction of oxidized In in the bimetallic particles and possibly to a further stabilization of this phase deriving from the interaction with Bi. Indium oxides and hydroxides metastable on the surface during electrolysis, in fact, have been shown to be the most selective phase for the reduction of CO_2 to formate. [5,6] We use this superior catalyst in a design of experiments (DOE) to optimize a GDE. For more details on the design of experiment and the resulting models, see the paper

on which this chapter is based. The best performing electrodes screened in this study show nearly 100% faradaic yield at current densities up to 400 mA/cm^2 for two hours. Moreover, we show one electrode to operate at a current density of 200 mA/cm^2 for 48 hours at a faradaic yield of 85% and to remain operating with a faradaic yield above 50% for 124 hours.

7.2 Experimental Section

7.2.1 Materials and chemicals. $InCl_3$ 99.999% and trisodium citrate dihydrate >99%, were purchased from Aldrich. Vulcan carbon (VXC72R) was purchased from Cabot Corp. Carbon cloth (60% Teflon treated) and Nafion^{TM} solution (5 wt% solution) were obtained from the Fuel Cell Store. $KHCO_3$ 99.5%, H_2SO_4 95% solution in water and $NaBH_4$ 98+% were purchased from Acros Organics. Triethylene glycol (TEG) 99% and $Bi(NO_3)_3{\cdot}5H2O$ 98% were purchased from Alfa Aesar. PVDF Kynar flex 2801 was purchased from Arkema.

7.2.2 Particle production and ink formulation. The carbon supported particles were prepared in TEG *via* a chemical reduction method. For the synthesis of the bimetallic InBi catalysts (50:50 wt %), 1.64 g of $InCl_3$ and 1.98 g of $Bi(NO_3)_3{\cdot}5H_2O$ were dissolved in 250 mL of triethylene glycol (TEG) along with 1.14 g of trisodium citrate dihydrate. The mixture was stirred and heated to 60 °C under a N_2 atmosphere until the salts were dissolved. Different amounts of Vulcan carbon were added, according to the desired metal loading on carbon (30, 60 or 90 wt%) and the mixture was stirred overnight. An overview of the different amounts of carbon can be found in Table 7.1. The resulting suspension was heated to 100 °C and the N_2 atmosphere was switched to an Ar atmosphere. When the desired temperature was reached, 4.5 mL of a 12.5 M $NaBH_4$ solution were added over 40 seconds. After this, the mixture was let to react for 15 minutes before being cooled down, filtered and washed several times with isopropanol and isopropanol/water mixtures.

For the single metals, a similar procedure was used: the reaction was scaled down to 100 mL and 1.1 g of $InCl_3$ were used for the In-only catalyst, while 2.4 g of $Bi(NO_3)_3 \cdot 5H_2O$ were used for the Bi-only catalyst. The amount of carbon was chosen so that the atomic % of metal on carbon, rather than the weight % on carbon, of the single metal catalyst would be similar to the 60 wt% InBi on carbon (53.7 wt% In on C and 67.9 wt% Bi on carbon).

The InBi catalysts with different loadings on carbon were used for the Design of Experiments (DOE), while the single metal catalysts were compared to the InBi 60 wt% on carbon for the benchmarking and characterization.

Two types of binders were investigated in this study: PVDF and Nafion™. The inks were formulated according to the used binder to be applied to the GDL. In the case of Nafion™, the catalysts were sonicated in isopropanol before the addition of the binder, while for PVDF a mixture of isopropanol and acetone was used as a solvent, to avoid the precipitation of the binder. Three different binder loadings were tested: 10, 20 and 30 wt% of dry binder in the catalyst layer. The amounts of binder added to the ink were chosen according to the catalyst weight in the ink.

The inks were airbrushed on home-made GDLs aiming to reach three different theoretical metal loadings: 0.5, 1.25 and 2 mg_{metal}/cm^2.

Catalyst	Composition	
	wt% on C	g Vulcan C
InBi/C	30	4.4
InBi/C	60	1.0
InBi/C	90	0.2
In/C	53.7	0.5
Bi/C	67.9	0.5

Table 7.1. Amounts of C used for synthesis.

7.2.3 Gas diffusion layer production. The synthesis method for the GDLs in this study was modified from a patented method.[7] 8.92 mL of PTFE DISP 30 was added to 70mL of a 1:1 volume IPA:water mixture and stirred for 1 minute before mixing with 15g of Soltex Acetylene black 75%-03 carbon in a Bourgini mixer. After 1 minute of mixing, a dough like mixture was collected. A rolling pin was used to prepare the dough for a cross rolling technique to obtain the desired thickness where the thickness setting is a discrete numerical factor. A rectangle about 250 cm^2 was cut from this structure and a paint roller was used to apply PTFE DISP 30 diluted 50% with 1:1 volume IPA:H_2O to the back of the dough. Fibreglast™ 1k plain weave carbon fiber fabric was used as the current collector and placed on top of the PTFE applied layer. A Carver heated press (Model number 4533) was used to press the structure in three stages at various temperatures, pressures, and durations according to the two GDL methods tested shown in Table 7.2. GDLs of 4.4 cm x 4 cm were cut from the final structures.

Production Process Condition	GDL 1	GDL 2
PTFE wt%	35	35
Rolling Thickness Setting	4	4
Time Stage 1 (min)	60	32.5
Pressure Stage 1 (Ton)	20	10.25
Temp Stage 1 (^oC)	200	140
Time Stage 2 (min)	60	32.5
Pressure Stage 2 (Ton)	20	10.25
Temp Stage 2 (^oC)	335	307.5
Time Stage 3 (min)	60	32.5
Pressure Stage 3 (Ton)	25	13
Temp Stage 3 (^oC)	335	317.5

Table 7.2. GDL Production Conditions

7.2.4 Electrochemical measurements. Cyclic voltammetry was carried out in a cell connected to a Bio-logic MPG2 potentiostat (with EC-lab software version 11.10). A leak free Ag/AgCl electrode was used as the reference electrode and the counter electrode was a Pt gauze. The working electrode was carbon cloth on which the catalytic ink was dropcasted. The electrolyte was a 0.5M $KHCO_3$ solution, saturated with either CO_2 or N_2 before running the experiments. The electrodes, with an exposed area of 1 cm^2 were cycled at a scan rate of 50 mV/s with N_2 or CO_2 continuously purging the headspace of the cell.

7.2.5 Particle characterization. X-Ray diffraction patterns of the particles supported on carbon were obtained by a Philips X'pert equipped with X'lerator in a 2Θ range from 20 to 80 degrees. SEM was performed on an Apreo SEM equipped with an energy dispersive X ray (EDX) analyzer. X-ray photoelectron spectroscopy measurements were performed on the catalyst powders with a Thermo Fisher K-alpha instrument. Differential scan calorimetry was performed on a Mettler Toled DSC 3+ Star^e System at a scan rate of 5 °C per minute between 25°C and 300°C for two times. The composition of the particles and the actual loading on the carbon support was investigate with Inductively Coupled Plasma spectroscopy (ICP).

7.2.6 Flow cell electrolysis. The electrolysis was carried out in a commercial three-compartment, 10 cm^2 GDE flow cell (ElectroCell Micro Flow Cell). The anode and the cathode were separated by a reinforced Nafion^{TM} membrane N324. The anolyte was a 0.5M H_2SO_4 solution and the anode catalyst was a Ti current collector coated with Ir/RuO_2, the anodic reaction was the oxygen evolution reaction (OER). The catholyte was a 0.5M $KHCO_3$ solution, the cathode was a GDE airbrushed with one of the synthesized catalysts. The electrolyte solutions were circulated in the compartments at a flow rate of 50 mL/min with a peristaltic pump, and CO_2 was fed through the GDE in the cathodic compartment at a flow rate of 50 to 100 mL/min, depending on the current. The cell was connected to a power supply and operated galvanostatically at different currents for different amounts of time. For the benchmark experiments (InBi compared to pure In and Bi) they were operated at 200 mA/cm^2 for 4 hours. For the DOE experiments, each electrode was operated at 200, 300 and 400 mA/cm^2 for 2 hours each in random order. Only the first applied current density was considered for the DOE.

Samples of the catholyte were collected, neutralized with HCl and analyzed for soluble products with a Perkin Elmer Lambda 35 UV-vis spectrometer.

7.2.7 Design of experiments for catalyst layer optimization. The Custom Design Platform in JMP was used to generate a DOE for this study to investigate the effect of the following parameters on the cell potential, FY towards formate, and electrode stability: GDL type, loading of metal catalyst, amount of catalyst supported on carbon, weight percentage of binder in the catalyst layer, binder type, and current density.[8] This resulted in 32 electrolysis experiments with different combinations of the above mentioned parameters. In this chapter, we only report the FY of each of the 32 experiments in Table 7.3. The interested reader can find an exhaustive discussion of the full statistical analysis in the paper from which this chapter is extracted.

7.2.8 Extended operation experiments. Two experiments were performed as extended operation runs to determine the lifetime stability of these electrodes. The two electrodes used for experimental run 5 (original run and repeat run) were used for these extended operation experiments. Therefore, each electrode for these experiments was operated for six hours in the DOE set prior to running the extended experiments. Each electrode was operated at a different constant current density until the faradaic yield of formate decreased below 50%. Additionally, every 24 hours the current to the electrochemical cell was set to zero, the cathode compartment was rinsed with deionized water, and air was passed through the cathode compartment for one hour before restarting the cell at the operating current density.[9]

7.3 Results

7.3.1 Flow cell electrolysis: benchmarking InBi against single metals. The performance of the InBi catalyst was benchmarked against In and Bi single metal catalysts by comparing the faradaic yield (FY) of the CO_2 electroreduction to formate at 200 mA/cm^2 for 4 hours. The catalyst layer was formulated with 20 wt% PVDF for these control experiments. The loading of catalyst applied to the GDL was chosen so that similar amounts (in mmol) of total metal would be present on the electrode in the case of InBi and the single metal catalysts. The results are summarized in Figure 7.1. The InBi catalyst is the best performing one with a FY of 96%, followed by 93% for In and 74% for Bi. This is in good agreement with the patented results[4] which show that, in bulk metal electrodes, InBi is slightly more selective than an anodized In electrode (80% vs 76% FY) and significantly more selective than non-anodized In (64% FY). In our case, In performs only slightly worse than the InBi catalyst. This may be caused by the fact that the particulate nature of the catalyst enhances the surface exposed, increasing the amount of oxide. The importance of metastable (hydr)oxides for the selectivity of In catalysts for CO_2 reduction to formate has been argued in previous studies.[5,6]

The overall enhancement of selectivity is probably attributable to the more favorable mass transport properties of the GDE configuration.

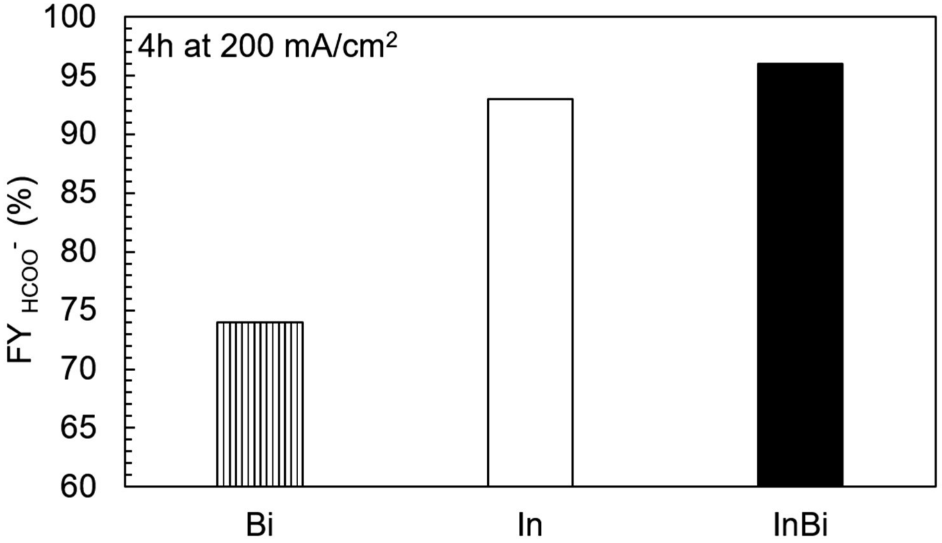

Figure 7.1. Comparison of faradaic yield of the single metal catalysts compared to the bimetallic InBi catalyst during 4 hours of operation at 200 mA/cm^2.

7.3.2 Catalyst characterization. The morphology and distribution of the particles on the carbon support was investigated with SEM. Some representative pictures are shown in Appendix E (Figure E1 and E2), where a comparison of the single metal catalysts and the InBi catalyst at a similar loading on carbon as well as a comparison of InBi catalysts at different loadings on carbon is shown. In the images, it is possible to see that with the exception of the InBi 30 wt% on carbon, the synthesis yields big particles, in the range of hundreds of nanometers, embedded (rather than supported) on the carbon support due to the big size.

The elemental composition and loading on carbon were investigated by ICP. The results are shown in Appendix E (Figure E3). While the amount of Bi on the carbon support is consistent with the expected one, In is lower in both the monometallic and bimetallic samples.

During the washing cycles a brown suspension was observed in the filtrate for the In and InBi catalysts, indicating that some of the metal is leached out. The actual loadings on carbon are 33% for In (53.7% expected), 63.6% for Bi (67.9% expected) and 55.4% for InBi (60% expected) with a weight ratio of In:Bi of 0.6 (expected ratio is 1). This gives a molar composition of approximately 50:50 In:Bi in the bimetallic catalyst (expected 65:35 In:Bi).

Figure 7.2 shows the results of our DSC analysis of the three catalysts. During the first cycle (Figure 7.2a), a broad feature before 100 °C is observed in all the catalysts and is attributed to the evaporation of residual moisture present in the sample. In and Bi show the characteristic melting point of the metallic phases (156°C for In and 271 °C for Bi), while the only significant peak in the InBi sample is the one attributable to metallic Bi. InBi only shows minor peaks related to bimetallic phases at 66°C, 84 °C and 107°C, which can respectively be attributed to the eutectic phase, the compound $BiIn_2$ and the compound BiIn.[10] The melting points are slightly shifted to lower temperatures compared to the expected ones of 72°C, 88°C and 109°C and this is possibly due to the existence of these compounds in very small crystalline domains, where the melting point depression effect starts to be significant.[11] A very small peak related to metallic indium (156 °C) is also visible.

During the second cycle (Figure 7.2b)) the DSC spectra are more flat and easily quantifiable, but, in the case of the InBi sample, all peaks related to InBi intermetallics and In have disappeared, indicating that exposure to high temperatures can decompose the residual weak In-Bi bonds in favor of the stronger In-O bonds. Even though the DSC chamber is kept under a stream of N_2 we expect this to be possible due to the presence of residual oxygen and water in the porous carbon matrix or its presence as oxidized carbon groups on the surface of the carbon support. The melting point of Bi is shifted to lower temperatures in the InBi catalyst compared to the pure Bi catalyst, and since In is not soluble in the Bi matrix, this is probably due to the existence of metallic Bi in small crystalline domains, rather than to the formation of solid solutions.

By integrating the peak areas and knowing the heats of fusion (3.27 kJ mol^{-1} for In and 11.3 kJ mol^{-1} for Bi) and the total amounts of metal in the samples, we can estimate the amount of metal present in the metallic state, assuming that the remaining part will be in an oxidized state. The oxides of In and Bi are not visible in the investigated temperature range since their melting points are higher than 300 °C. During the first cycle, in the InBi sample, only 4% of the In is present in the metallic state. The intermetallic compounds, not knowing the exact heats of fusion, are impossible to quantify, but the total amount of energy exchanged during their fusion is very small, indicating that only a minor amount of these compounds is present. During the second cycle, the amount of metallic Bi is 60.9% in the pure Bi particles and 56.9% in the InBi particles. The amount of metallic In is 54.5% in the pure In particles and 0% in the InBi particles, indicating that all the In present is in the oxide form. Therefore, it seems that the presence of Bi can enhance the oxidizability of In rather than forming intermetallic compounds in our particles, at least after air exposure. This can be explained by the different electronegativity of In and Bi (1.78 vs 2.02). Since Bi is a more noble metal, it could be favoring the oxidation of In in a galvanic corrosion process.

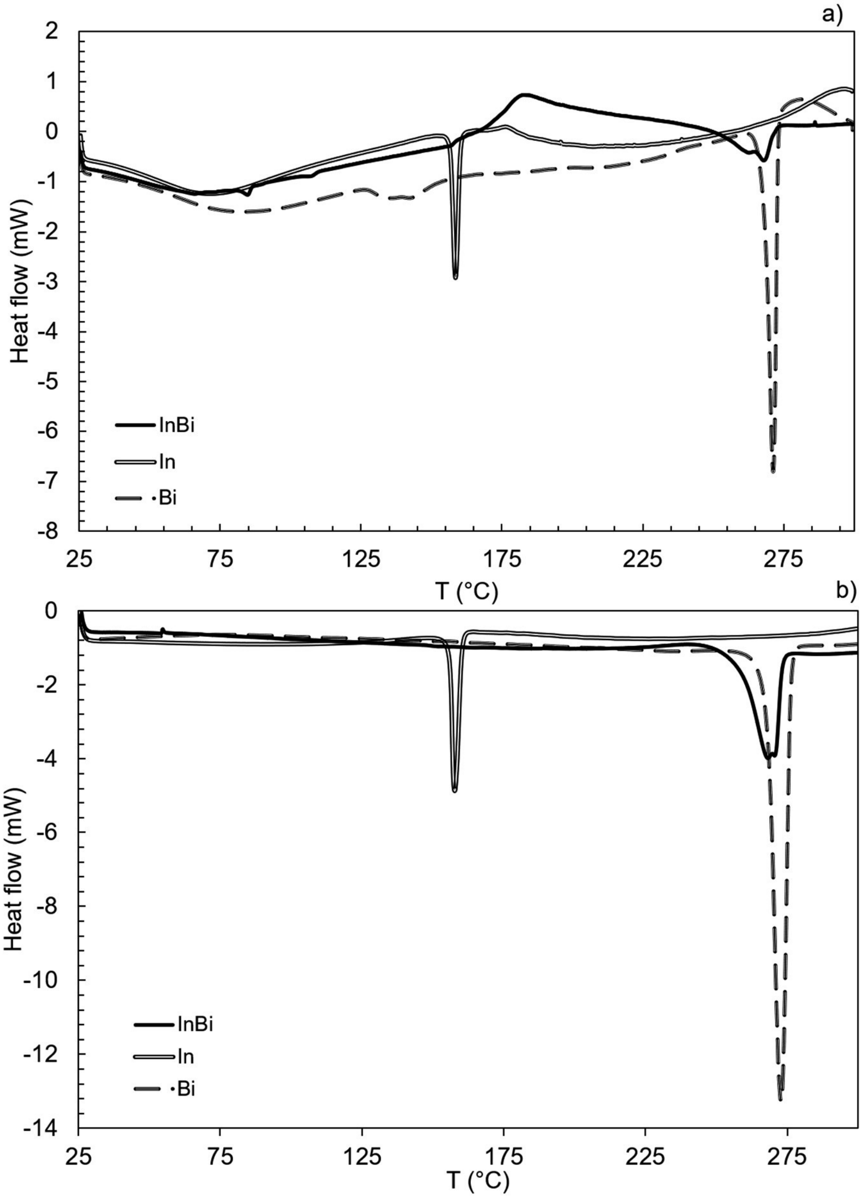

Figure 7.2. Differential scanning calorimetry of pure In, pure Bi and InBi particles supported on carbon. a) first cycle and b) second cycle.

The results of the XPS analysis (Figure 7.3) confirm the surface enrichment and oxidation of In. In fact, in both the pure In and InBi particles, the species In^{3+} makes up 98-99% of observed In. Moreover, while the elemental composition from ICP indicates an overall atomic composition of 50:50 in the InBi particles, the XPS atomic ratios are 80.5% In and 19.5% Bi, indicating that the first few nanometers of the particles are indium-enriched. Also, with the large majority of the In being detected in the oxidized form, it is probable that the residual intermetallic compounds detected during the first DSC cycle would be buried in the inner parts of the particle. The In peaks in the InBi particles are shifted positively of 0.2 eV compared to those in the pure In particles, possibly due to the electron withdrawing effect of the more electronegative Bi atoms, which in turn would increase the oxidizability of In. The behavior of the Bi XPS spectrum is somewhat more complex. The Bi peaks in the InBi catalyst are broadened and shifted to higher binding energy compared to the pure Bi catalyst, which would be counterintuitive if we expect the Bi atoms to simply bear the partial negative charge drawn from the In. Such an effect could be caused, for example, by the dispersion of Bi in the In oxide matrix in the form of single atoms or small clusters (like suggested by the DSC results), which would add layers of complexity to the overall photoemission behavior, compared to the bulk Bi to which it is compared. Similar shifts in XPS spectra with decreasing particle size have been observed before.[6] Since the Bi results may be difficult to deconvolute and interpret correctly, its XPS spectra were used only for the calculation of the atomic ratios.

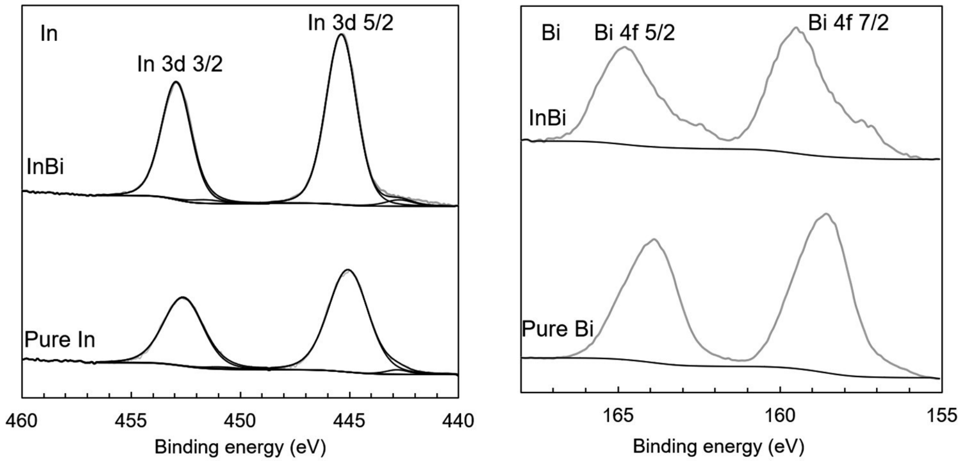

Figure 7.3. XPS of In (left) and Bi (right) in pure metal particles (bottom line) and InBi particles (upper line). While the deconvolution into In^{3+} and In(0) is shown, the raw spectra are shown in the case of Bi, since only the peak area could be used for the atomic concentration calculations.

The X-ray diffraction patterns of the three materials are shown in Figure E4, in Appendix E. Despite the DSC analysis showing that a significant fraction of the elements is present as oxides, only reflections relative to the elements in their metallic state can be seen in the diffraction patterns, indicating that the oxides on the surface may be amorphous. In particular, only a small reflection for metallic In is seen in the InBi particles, while all the other peaks can be assigned to metallic Bi. The diffraction peaks in the InBi pattern are not significantly shifted with respect to the pure metals, indicating that the two elements are not forming solid solution phases in their metallic state. Moreover, no reflections assignable to the intermetallic phases are observed. This is consistent with the hypothesis of the melting point depression of the residual intermetallic phases being due to the small size of the domains, which would result in them being XRD amorphous. It could also be caused by the extremely small amounts present. In addition to this, the metallic Bi peaks are broadened compared to the pure Bi particles, supporting the idea that Bi is present in small domains dispersed in a matrix composed mostly of amorphous In oxide.

7.3.3 Electrochemical measurements. The three catalysts were cycled several times in N_2 and CO_2 saturated 0.5M $KHCO_3$ at 50 mV/s. Figure 7.4 shows the voltammograms. The comparison of the voltammetries of the three catalysts in N_2 and CO_2 saturated electrolyte is instead shown in Appendix E (Figure E5a and E5b).

It is easily noticeable that, qualitatively speaking, the cyclic voltammogram of the InBi catalyst is very similar to the one of In. The redox features of Bi, and especially the reduction peak around -0.7V vs Ag/AgCl, which is a prominent feature in the voltammetry of pure Bi, are barely noticeable. This suggest that the surface of the particles is mainly composed of In, in accordance with the XPS data. The XPS shows that 80.5% of the atoms in the first few nanometers are indium atoms, but with the cyclic voltammetry we can see that the electroactive surface is likely even more enriched in In. Therefore, during CO_2 reduction, the surface is probably composed of a large amount of In, with a small number of Bi inclusions.

Aside from the features related to the metallic surface of the electrode, it is interesting to compare the behavior of the catalysts in the cathodic branch where hydrogen evolution and CO_2 reduction are expected to happen. The overlayed cyclic voltammetries of the three catalysts in N_2 and CO_2 saturated electrolyte are shown in Appendix E (Figure E5a and b). It is clear that the behavior of the InBi catalyst in this cathodic region is very similar to the one of pure In, suggesting that In itself is the main contributor to the CO_2 reduction (or hydrogen evolution) behavior, while Bi seems to slightly enhance its performance in the case of CO_2 reduction.

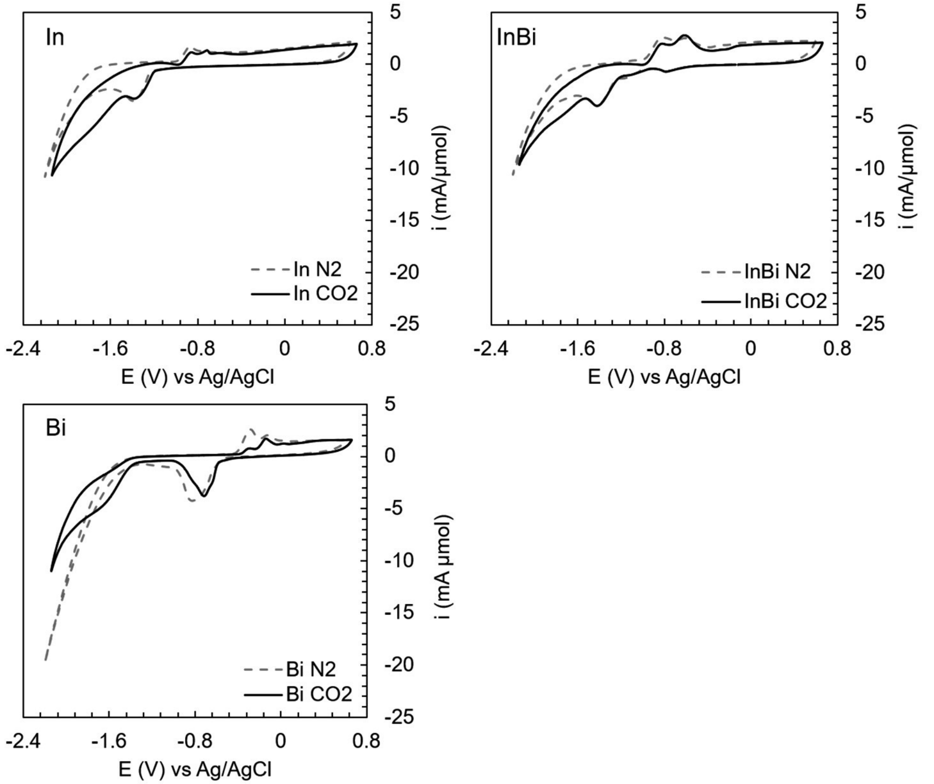

Figure 7.4. Cyclic voltammograms of In, Bi and InBi in CO_2 saturated 0.5M $KHCO_3$ (solid black lines) and N_2 saturated 0.5M $KHCO_3$ (dashed gray lines).

7.3.4 Design of experiments. The tabulated DOE results are shown in Table 7.3. In this chapter, they are simply intended to summarize the investigated parameters and the FY response. For the full analysis in JMP, we direct the interested reader to the full paper.

Run	GDL Method	Loading (mg/cm^2)	Catalyst on Carbon (wt%)	Current Density (mA/cm^2)	Binder in Catalyst Layer (wt%)	Binder Type	Formate faradaic yield
1	1	2	30	400	30	PVDF	68.5%
2	1	0.5	30	400	10	PVDF	93.5%
3	1	1.25	90	300	10	PVDF	69.9%
4	2	2	30	400	30	Nafion ™	84.1%
5	1	2	60	400	20	PVDF	94.6%
6	1	0.5	30	400	20	Nafion ™	83.5%
7	2	2	90	300	20	Nafion ™	93.4%
8	1	2	90	400	10	Nafion	94.2%
9	1	2	60	200	30	Nafion ™	82.4%
10	2	2	90	400	30	PVDF	28.2%
11	1	0.5	90	400	30	PVDF	23.4%
12	2	0.5	90	200	30	PVDF	86.3%
13	1	2	30	300	10	Nafion ™	84.6%
14	2	1.25	60	400	10	Nafion ™	77.2%
15	2	0.5	90	400	10	PVDF	60.0%
16	2	0.5	30	400	30	PVDF	93.1%

17	2	0.5	30	200	10	PVDF	90.3%
18	2	0.5	30	300	10	Nafion ™	87.4%
19	2	0.5	30	200	30	Nafion ™	79.7%
20	1	0.5	60	300	30	Nafion ™	40.2%
21	2	2	90	200	10	PVDF	88.5%
22	1	2	90	200	30	PVDF	23.3%
23	2	2	30	200	30	PVDF	85.4%
24	1	0.5	90	200	10	Nafion ™	95.4%
25	1	1.25	30	200	20	Nafion ™	94.1%
26	2	1.25	90	200	30	Nafion ™	70.3%
27	2	2	60	200	10	Nafion ™	95.2%
28	1	0.5	30	200	30	PVDF	86.1%
29	1	2	30	200	10	PVDF	77.1%
30	2	0.5	90	400	20	Nafion ™	99.4%
31	2	2	30	400	10	PVDF	63.4%
32	1	1.25	90	400	30	Nafion ™	13.4%

Table 7.3. Experimental Design Matrix and Run Results

7.3.5 Extended operation experiments. Electrodes used from run number 5 (Table 7.3) were used for the extended operation experiments. Each electrode used was ran in the DOE for six hours before operating in the extended run experiments. Separate electrodes were operated at different current densities for these extended experiments. A plot of the FY vs time for the two electrodes is shown in Figure 7.5.

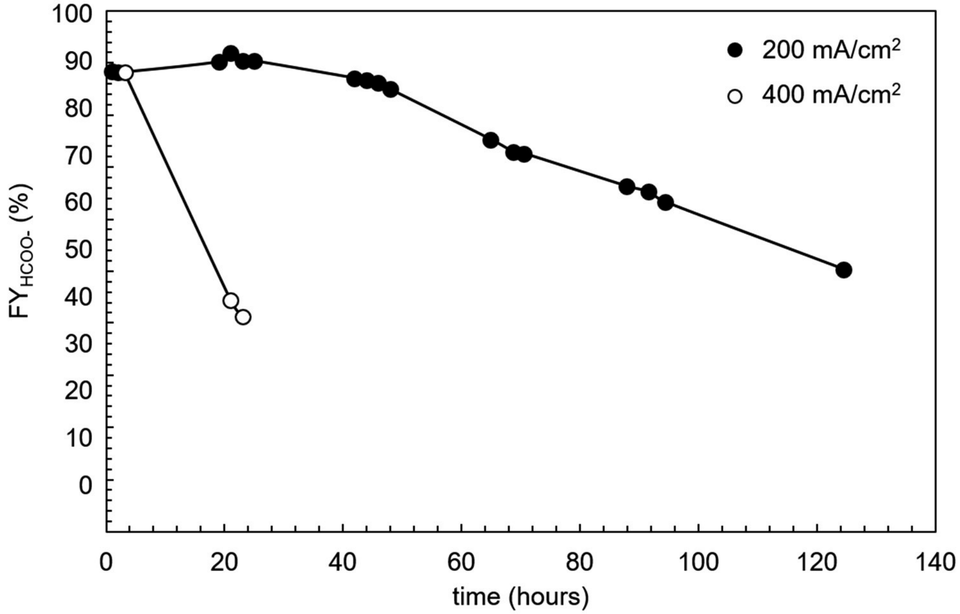

Figure 7.5. FY toward formate vs time for two electrodes operated for extended hours

7.4 Discussion

7.4.1 Catalyst physicochemical characterization. While it is possible that during the synthesis of the particles some intermetallic compounds may be formed in accordance with the phase diagram of the In-Bi system,[10] it appears that exposure to the atmosphere will cause the In fraction of the particles to segregate on the surface. This is due to the extremely weak bonds formed between In and Bi, as shown by the only slightly exothermic enthalpies of formation of their intermetallic compounds,[12] and by the larger tendency of In to be oxidized (ΔH_f^0 Bi_2O_3 = -573.9 kJ mol^{-1} versus ΔH_f^0 In_2O_3 = -925.8 kJ mol^{-1}). Also, the percentage of In in its oxidized state is significantly higher in the InBi particles compared to the pure In particles (in fact, most of the In is oxidized in InBi particles, as opposed to around 50% in pure In particles), suggesting that the presence of Bi is somehow enhancing this process of oxidation, as would be expected by the different electronegativity of the elements. Coupling metals with significantly different redox potentials, in fact, can cause an increase in the rate of oxidation of the least noble one, a process known as galvanic corrosion. The cyclic voltammetry of InBi shows predominantly features related to In, both in the metal redox peaks and in the cathodic branch, confirming that the electrochemically active surface area is predominantly composed of this element (as also supported by our XPS analysis). With this evidence, we propose that the effect of the presence of Bi in our bimetallic InBi particles is similar to an anodization process, which has been shown in the literature to improve the selectivity of In catalysts.[6] Moreover, it is possible that the electron withdrawing effect of Bi on In could partially increase the stability of metastable In oxides, enhancing their presence on the surface during electrolysis and thereby slightly increasing the selectivity of this catalyst compared to a pure In one.

7.4.2 Design of experiments. It is clear from Table 7.3 that the formulation of the catalyst layer can have a profound effect on the selectivity of the system, despite the high selectivity shown by the InBi catalyst in optimal conditions. The most important factor is the wt% of binder in the catalyst layer, where too much binder can lower CO_2 reduction activity by blinding active sites and too little binder can cause mechanical weakness of the catalyst layer. In particular, the optimum amount of binder depends on the catalyst loading on carbon and the GDL type employed. Surprisingly, in our system, the type of binder does not seem to have a significant influence on the performance, suggesting that in our case the binder's most important function is to hold the catalyst layer together, rather than providing ionic

conductivity. In fact, while Nafion™ is a good proton conductor, PVDF is not an ionomer.

The best performing experiment, run 30, employed a catalyst layer composed of 90wt% InBi/C bound with 20wt% Nafion™, at a loading of 0.5 mg_{metal}/cm^2 on GDL type 2. The FY was 99.4% at 400 mA/cm^2.

7.4.3 Extended operation experiments. The electrode operated at 200 mA/cm^2 achieved 130.5 hours of total operation (including the hours of operation from the DOE experiment) above 50% FY toward formate. Additionally, this electrode operated above 85% FY toward formate for nearly 54 hours. On the other hand, the electrode that was ran at 400 mA/cm^2 dropped drastically in FY toward formate in less than 27 hours of total operation. This shows that the current density can extremely affect the lifetime of these electrodes.

7.5 Conclusions

In conclusion, we have shown that InBi catalysts prepared with our method are slightly more selective than In catalysts and markedly more selective than Bi catalysts prepared with the same method. This effect seems to be due to the fact that Bi, in a process that may be similar to galvanic corrosion, increases the fraction of In in its oxidized state, a process that induces the segregation of this metal to the surface of the particles. The particles with a surface enriched in indium oxides, in turn, would increase the selectivity since this phase has been shown to be the most active for CO_2 reduction to formate.

Moreover, we optimized a GDE for this reaction by using a DOE to identify crucial factors and interactions that affect the FY toward formate. Nearly one third of the GDEs produced for these experiments achieved over 90% FY toward formate at current densities ≥ 200 mA/cm^2. The binder amount in the catalyst layer affects the FY toward formate the most with the InBi catalyst. There appears to be an optimal binder amount that is dependent on the amount of catalyst supported on carbon and the GDL used.

Finally, the stability of the electrode was assessed by operating two of the same electrodes at different current densities until the FY toward formate decreased below 50%. The two electrodes operated for extended hours were DOE experiment number five electrodes. One electrode operated at 200 mA/cm^2 above 50% FY for an additional 124.5 hours. However, the other electrode, operated at 400 mA/cm^2 ran for less than 24 additional hours before the FY toward formate decreased to below 50%. This shows that the operating current density considerably affects the lifetime of the electrodes. In the future, it will be important to look at several factors affecting the lifetime and stability of the electrodes to potentially find ways to operate for longer, at current densities greater than 200mA/cm^2.

References

(1) Hori, Y. Electrochemical CO_2 Reduction on Metal Electrodes, Modern Aspects of Electrochemistry. 2008, 89–189.

(2) Higgins, D., Hahn, C., Xiang, C., Jaramillo, T. F. & Weber, A. Z. Gas-Diffusion Electrodes for Carbon Dioxide Reduction: A New Paradigm. *ACS Energy Lett.*, 2019, 4, 317–324.

(3) Philips, M. F., Gruter, G.-J. M., Koper, M. T. M. & Schouten, K. J. P. Optimizing the Electrochemical Reduction of CO_2 to Formate: A State-of-the-Art Analysis. *ACS Sustain. Chem. Eng.*, 2020, 8, 15430–15444.

(4) Parajuli, R., Ansovini, D., Philips, M. F. & Schouten, K. J. P. Catalyst system for catalyzed electrochemical reactions and preparation thereof, applications and uses thereof. International Publication Number WO 2019/141827 A1.

(5) Pander, J. E., Baruch, M. F. & Bocarsly, A. B. Probing the Mechanism of Aqueous CO_2 Reduction on Post-Transition-Metal Electrodes using ATR-IR Spectroelectrochemistry. *ACS Catal.*, 2016, 6, 7824–7833.

(6) Detweiler, Z. M., White, J. L., Bernasek, S. L. & Bocarsly, A. B. Anodized indium metal electrodes for enhanced carbon dioxide reduction in aqueous electrolyte. *Langmuir*, 2014, 30, 7593–7600.

(7) Philips, M. F., Ansovini, D., Figueiredo, M. C. C. & Krasovic, J. Method for the Preparation of a Gas Diffusion Layer and a Gas Diffusion Layer Obtained or Obtainable by Such Method. 2020,.

(8) SAS Institute Inc. JMP^{TM} 14 Design of Experiments Guide. 2018, 241–294.

(9) Ansovini, D., Philips, M. F., Krasovic, J., Figueiredo, M. C. C. & Schouten, K. J. Formation of Formic Acid with the Help of Indium-Containing Catalytic Electrode. 2021,.

(10) Okamoto, H., Schlesinger, M. E. & Mueller, E. M. Bi (Bismuth) Binary Alloy Phase Diagrams. *Alloy Phase Diagrams* 2016, vol.

3 0.

(11) Allen, G. L., Bayles, R. A., Gile, W. W. & Jesser, W. A. Small particle melting of pure metals. *Thin Solid Films*, 1986, 144, 297–308.

(12) Kulikova, T., Mayorova, A., Shubin, A., Bykov, V. & Shunyaev, K. Bismuth-indium system: Thermodynamic properties of liquid alloys. *Kov. Mater.*, 2015, 53, 133–137.